COMMUNICATION

Magnetic Resonance in Medicine 57:639–646 (2007)

Rapid Quantitation of Cardiovascular Flow Using Slice-Selective Fourier Velocity Encoding with Spiral Readouts

Joao L. A. Carvalho and Krishna S. Nayak

Accurate flow visualization and quantitation is important for the assessment of many cardiovascular conditions such as valvular stenosis and regurgitation. Phase contrast based methods experience partial volume artifacts when flow is highly localized, complex and/or turbulent. Fourier velocity encoding (FVE) avoids such problems by resolving the full velocity distribution within each voxel. This work proposes the use of slice selective FVE with spiral readouts to acquire fully localized velocity distributions in a short breath-hold. Scan-plane prescription is performed using classic protocols, and an automatic algorithm is used for in-plane localization of the flow. Time and spatially-resolved aortic valve velocity distributions with 26-msec temporal resolution and 25 cm/sec velocity resolution over a 600 cm/sec field-of-view were acquired in a 12-heartbeat breath-hold. In carotid studies, scan time was extended to achieve higher spatial resolution. The method was demonstrated in healthy volunteers and patients, and the results compared qualitatively well with Doppler ultrasound. Acquisition time could be reduced to 7 heartbeats (a 42% reduction) using partial Fourier reconstruction along the velocity dimension. Magn Reson Med 57:639–646, 2007. © 2007 Wiley-Liss, Inc.

Key words: MRI flow imaging; Fourier velocity encoding; valvular disease; partial *k*-space reconstruction; stenosis; regurgitation

Accurate flow visualization and quantitation is important for the evaluation of many cardiovascular conditions, including valvular abnormalities, congenital defects, and coronary artery disease. Doppler ultrasound is the current gold standard for vascular and cardiac flow imaging. However, evaluation by ultrasound is inadequate when there is air, bone, or surgical scar in the acoustic path, and flow measurement is inaccurate when the ultrasound beam cannot be properly aligned with the axis of flow (1,2). Magnetic resonance imaging (MRI) is a modality uniquely capable of imaging all aspects of heart disease and is a potential "one-stop-shop". The evaluation of valvular disease and intracardiac flow will be a necessary capability in a comprehensive cardiac MR examination.

In MR flow imaging, speed is of particular importance, as low temporal resolution may cause underestimation of peak velocities, and acquisition time is typically limited to the duration of a breath-hold. The most widely used method is phase contrast (3), in which scan time can be reduced by sacrificing temporal and spatial resolution. However, data inconsistency, partial-volume effects, and intravoxel phase dispersion can lead to the loss of diagnostic information (4,5). Fourier velocity encoding (FVE) shows satisfactory agreement with Doppler ultrasound (6) and is more accurate than phase contrast in visualizing and quantifying localized high-speed flow jets and complex or turbulent flow patterns, as it fully resolves the velocity distribution within each voxel, eliminating partial-volume problems (7). However, it may require considerably greater data collection.

Different approaches to accelerating FVE have been proposed, such as the use of two-dimensional cylindrical excitation to restrict the field-of-view to a beam that can be imaged without phase encoding (8–10). This approach allows spatial encoding and velocity encoding to be performed simultaneously in a single pulse repetition time (TR), but has problems related to the precise placement of the imaging beam, especially when the region of interest (e.g., aortic valve) moves during the cardiac cycle. Other problems include the large voxel size, which is limited by the readout trajectory, by the minimum achievable cylindrical excitation radius, and by patient safety limits and/or gradient heating, which also limit the minimum TR and thus the maximum temporal resolution.

Slice-selective FVE has been accelerated by performing spatial encoding along the readout direction only (11,12), or by acquiring velocity images with no spatial encoding other than slice selection (13). However, these techniques have dynamic range problems, as the signal of flowing blood has to be distinguished from all the background signal from static tissue. Furthermore, since the velocity measurement is a projection along the line or plane being imaged, this approach is unable to resolve different sources of flow that may coexist in that line or plane. Slice-selective FVE with 2D-resolved spatial encoding would provide easy localization of the region of interest, and the ability to automatically resolve multiple sources of through-plane flow in the imaged field-of-view, without requiring static tissue suppression.

We propose the use of slice-selective FVE with spiral acquisitions to acquire fully localized, time-resolved

Magnetic Resonance Engineering Laboratory, Department of Electrical Engineering–Systems, University of Southern California, Los Angeles, California.

Grant sponsor: National Institutes of Health; Grant number: HL074332; Grant sponsor: American Heart Associations; Grant number: 0435249N; Grant sponsor: GE Healthcare.

*Correspondence to: Joao L. A. Carvalho, USC Electrical Engineering–Systems, 3740 McClintock Ave, EEB 412, Los Angeles, CA 90089 - 2564, USA. E-mail: jcarvalh@usc.edu

Received 21 June 2006; revised 22 November 2006; accepted 1 January 2007.

DOI 10.1002/mrm.21196

Published online in Wiley InterScience (www.interscience.wiley.com).

velocity distributions in a short breath-hold. Scan-plane prescription is performed using classic protocols, and a semiautomatic algorithm is used for in-plane localization of the flow. The method was demonstrated in vivo, and the results were qualitatively compared with Doppler ultrasound. Patient results show that this technique can detect flow distributions in stenotic jets.

Without acceleration, spiral FVE can acquire cardiac velocity distributions in 12 heartbeats, with 26-msec temporal resolution and 25 cm/sec velocity resolution over a 600 cm/sec field-of-view, using single-shot spiral readouts. This time-velocity resolution is sufficient for the diagnostic assessment of valvular stenosis, where peak velocities are on the order of 200–600 cm/sec. The breath-hold duration can be reduced to 7 heartbeats by using partial Fourier reconstruction (14) along the velocity dimension. The velocity field-of-view, and/or the temporal, spatial and velocity resolutions can be improved by increasing the acquisition time. For example, in carotid studies scan time was increased to 48 heartbeats (without breath-hold) to achieve greater spatial resolution, by using multiple spiral interleaves.

THEORY

Fourier velocity encoding involves Fourier encoding along a velocity dimension (7). The velocity variable is v, the velocity frequency variable is $k_v = \frac{\gamma}{2\pi} M_1$, where γ is the gyromagnetic ratio, and M_1 is the first moment of a bipolar flow-encoding gradient aligned with the direction of the flow. Several velocity encoding levels (in our case, 16 or more) are used, typically by acquiring multiple images using different bipolar gradient amplitudes (and thus, different first moment values). This is equivalent to phase-encoding along k_v. An image acquired with a particular value of k_v is denoted $S_{x,y}(k_v)$. For a specific voxel (x, y), this represents one sample from the Fourier transform of the velocity distribution of all spins in the voxel. The voxel velocity distribution is denoted $s_{x,y}(v)$, and is obtained by inverse Fourier transformation along k_v. Placing the bipolar gradient along the z-axis will encode through-plane velocities. Placing the bipolar gradient along x or y will encode in-plane velocities. Oblique flow can be encoded using a combination of bipolar gradients along the x, y, and z axes.

METHODS

Scanner Setup

Experiments were performed on a GE Signa 3T EXCITE HD system, with gradients capable of 40 mT/m amplitude and 150 T/m/sec slew rate, and a receiver with sampling interval of 4 μsec. Sequence designs were optimized for this scanner configuration. The body coil was used for RF transmission in all studies. An eight-channel phase array cardiac coil was used in cardiac studies, but data from only one or two elements were used in reconstruction. Similarly, a four-channel neck coil was used in carotid studies, with only two channels used in reconstruction. In patient scans, a GE Signa 1.5T LX system with the same gradient and receiver configuration was used, and acquisition was performed using a 5-inch surface coil. The institutional review boards of the University of Southern California and Stanford University approved the imaging protocols. Subjects were screened for magnetic resonance imaging risk factors and provided informed consent in accordance with institutional policy.

Imaging

Pulse Sequence

The spiral FVE imaging pulse sequence (Fig. 1) consists of a slice-selective excitation, a velocity-encoding bipolar gradient, a spiral readout, and refocusing and spoiling gradients. The dataset corresponding to each temporal frame is a stack-of-spirals in k_x, k_y, k_v space (Fig. 2). The bipolar gradient effectively phase-encodes in k_v, while each spiral readout acquires one "platter" in k_x, k_y.

The excitation achieved a 5-mm slice thickness and 10° flip angle, with a 0.5-msec RF pulse and 1-msec gradient. Through-plane velocity encoding was implemented using a large bipolar pulse along the z direction that was scaled to achieve different k_v encodings. The velocity resolution is determined by the first moment of the largest bipolar gradient, and the velocity field-of-view is determined by the increment in the first moment for different velocity encodes. A bipolar duration of 2.5 msec achieves a velocity resolution of 25 cm/sec. Gradient duration increases if velocity resolution is improved.

In cardiac scans, an 8.1-msec optimized uniform-density single-shot spiral acquisition (15) acquires k_x, k_y at each velocity encode, and zeroth and first moments are refocused in 0.5 msec. The readout and refocusing gradients were designed using free software developed by Hargreaves (http://www-mrsrl.stanford.edu/~brian/vdspiral/). A 0.65-msec spoiling gradient (16) achieves a 6π phase-wrap over the slice thickness. The spoiling gradient was not overlapped with the refocusing gradients, but this could be done to further shorten the TR. In carotid scans, spatial resolution was increased by segmenting the k_x, k_y acquisition in four spiral interleaves, across extended scan time. In this case, the spiral readout and refocusing gradients durations are 7.6 and 0.9 msec,

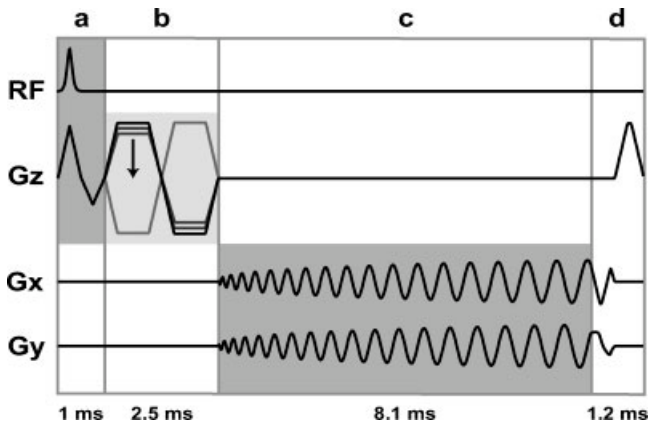

FIG. 1. Spiral FVE pulse sequence. It consists of (**a**) slice selective excitation, (**b**) velocity encoding bipolar gradient, (**c**) spiral readout, and (**d**) refocusing and spoiler gradients. This timing corresponds to the healthy volunteer cardiac studies in Figs. 3, 5, and 7.

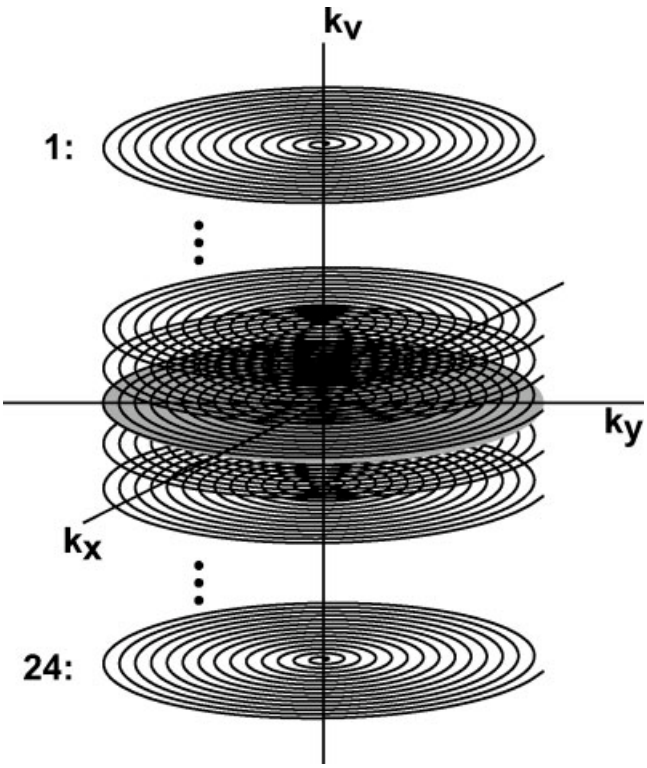

FIG. 2. Spiral FVE k-space sampling scheme. The dataset corresponding to each temporal frame is a stack-of-spirals in k_x, k_y, k_v space. Each spiral acquisition corresponds to a different k_v encode.

respectively. Total acquisition time in this case is four times longer, and breath-holding was not used. The minimum TR (≈13 msec) was used in all studies. Other scan dependent pulse sequence parameters are listed in Table 1.

Timing of Acquisitions

Prospective ECG gating was used to synchronize acquisitions with the cardiac cycle. In cardiac studies, two k_v levels were repeatedly acquired during each R-R interval in order to resolve 25–35 cardiac phases and produce a cine dataset (Fig. 3, discussed later). In carotid studies, one k_v level was acquired per heartbeat, and the spiral interleaves were segmented across multiple heartbeats using a sequential interleaf order. The true temporal resolution was 26 msec (2 TRs). Sliding window reconstruction was used to produce a new image every 13 msec.

Reconstruction

Reconstruction was performed in Matlab (Mathworks, South Natick, MA). Each spiral interleaf is first gridded (17) and inverse Fourier transformed to form an image x, y for each temporal frame. This step converts the acquired data $S_{k_x,k_y}(k_v, t)$ to $S_{x,y}(k_v, t)$. The operator manually defines a region of interest (ROI) in the x, y plane using the image corresponding to $k_v = 0$ and $t = 0$. Pixel intensities within the ROI are averaged at each temporal frame, resulting in a 2D dataset: $S_{\text{ROI}}(k_v, t) = \sum_{x,y}^{\text{ROI}} S_{x,y}(k_v, t)$. View-sharing is then applied to $S_{\text{ROI}}(k_v, t)$ to increase the number of temporal frames (18). Saturation effects (19) are compensated by dividing each $S_{\text{ROI}}(k_v, t)$ by the total energy at that temporal frame. This effectively normalizes each temporal frame. In carotid studies, signal from static tissue was discarded by subtracting the average value of $S_{\text{ROI}}(k_v, t)$ (along k_v) from all temporal frames. $S_{\text{ROI}}(k_v, t)$ is then zero-padded along the k_v axis, and an inverse Fourier transform produces $s_{\text{ROI}}(v, t)$. The time-velocity histogram for the ROI is $|s_{\text{ROI}}(v, t)|$, and for display purposes, smoother histograms are obtained by interpolating along t (20). Note that in carotid studies, which use multiple interleaves, view-sharing is applied prior to gridding.

The reconstruction process can be repeated for each voxel, or for multiple regions of interest, using the same data. The operator can be presented with a 2D color-overlay image or video indicating voxels where high-speed flow was detected, and use that as reference to select the regions of interest (see Fig. 6, discussed later). In our implementation, the operator manually defines a large ROI over the heart or around the carotid artery, and the best pixels within this ROI are selected to maximize the cost function

$$\max_{x,y} \frac{\int_{|v|\geq v_1} \int_{t=0}^{RR/2} |s_{x,y}(v,t)|^2 \, dt \, dv}{\int_{|v|\leq v_2} \int_{t=0}^{RR/2} |s_{x,y}(v,t)|^2 \, dt \, dv}, \qquad [1]$$

where v_1 and v_2 are thresholds that define ranges of high and low velocities, respectively. In other words, the algorithm selects the pixels that maximize the ratio between the energy at high velocities and the energy at low velocities, during the first half of the cardiac cycle. This cost function can be adjusted for different velocity ranges, or for different portions of the cardiac cycle. For example, to detect regurgitant jets, a modified cost function that locates high negative velocities during the second half of the R-R interval is:

$$\max_{x,y} \frac{\int_{v\leq -v_1} \int_{t=RR/2}^{RR} |s_{x,y}(v,t)|^2 \, dt \, dv}{\int_{|v|\leq v_2} \int_{t=RR/2}^{RR} |s_{x,y}(v,t)|^2 \, dt \, dv}. \qquad [2]$$

Experimental Methods

The proposed method was evaluated in vivo, aiming at quantifying flow through the common carotid artery and the aortic valve. Scan-plane prescription was performed

Table 1
Scan Parameters Used in the Different Studies

	Carotid	Cardiac (Healthy)	Cardiac (Patient)
Spiral interleaves	4	1	1
Field-of-view (cm)	20	25	20
Spatial resolution (mm)	2.5	7	6.5
Velocity field-of-view (cm/sec)	400	600/800	1200
Velocity encodings	24	24	32
Velocity resolution (cm/sec)	16.7	25/33	37.5
TR (msec)	13.2	12.8/12.5	12.8
k_v encodings/heartbeat	1	2	4
Interleaves/heartbeat	2	1	1
Temporal resolution (msec)	26.4	25.6/25	51.2
Scan time (heartbeats)	48	12	8

using a real-time imaging sequence, and in-plane localization of the flow was performed using the semiautomatic algorithm described earlier. The velocity field-of-view was chosen based on the targeted region of the body. For a severely stenosed heart valve, peak velocities can reach up to 600 cm/sec (13). In the carotid arteries, peak velocities are slightly lower, reaching up to 400 cm/sec. As regurgitant jets do not overlap in time with forward flow, we used 600 and 400 cm/sec as the velocity field-of-view for imaging the aortic valve and the carotids, respectively. These values could be increased by extending the scan time, or by sacrificing temporal, velocity and/or spatial resolutions. Scan parameters are summarized in Table 1.

Two experiments were performed to determine the appropriate view-ordering and interleaf-ordering schemes for both cardiac and carotid studies. In the first experiment, flow was measured through the aortic valve of a healthy volunteer, using one velocity encode level per heartbeat, with a single-shot spiral readout, and over a 24-heartbeat breath-hold. During reconstruction, 50% of the data was discarded in two different ways, to simulate the sequential and interleaved view-ordering schemes and to compare resulting artifacts. In the second experiment, flow was measured through the carotid artery of another healthy volunteer, using a 4-interleaf spiral FVE acquisition. The measurement was performed twice, and in each acquisition, a different view-ordering scheme was used. In the first acquisition, one spiral interleaf was acquired per heartbeat, and two different k_v levels were encoded throughout each R-R interval. In the second acquisition, two spiral interleaves were acquired per heartbeat, encoding one k_v level per cardiac cycle. Reconstructed velocity histograms were compared with respect to data inconsistency artifacts related to view-ordering.

In cardiac and carotid experiments, Doppler ultrasound was used as a "gold standard" and was qualitatively compared with the proposed method. Carotid flow was studied in three healthy subjects. Aortic outflow (at the valve plane) was studied in seven volunteers and two patients with aortic stenosis.

The feasibility of reducing scan time using partial-Fourier acquisition was tested using data from volunteer and patient studies. In each case, up to 42% of the acquired data (along k_v) was discarded and then synthesized using homodyne reconstruction (14).

RESULTS

Results from the cardiac view-ordering experiment are shown in Fig. 3. When the k_v levels are acquired in a sequential fashion, ghosting artifacts due to data inconsistency appear shifted by 1/2 of the velocity field-of-view (Fig. 3a). When they are acquired in an interleaved fashion, the artifacts overlap with the true flow profile (Fig. 3b), blurring the velocity histogram and making the detection of the peak velocity and other flow related parameters less precise. Using the sequential ordering and an appropriate velocity field-of-view, the artifacts will not overlap with the flow profile and may be easily identified and masked out. Thus, we used the sequential view-ordering in all subsequent cardiac acquisitions.

The results from the carotid view-ordering experiment are shown in Fig. 4. It can be noticed that the ghosting artifacts that arise in the velocity histograms when acquiring two different velocity encode levels during the same heartbeat (Fig. 4a) did not appear when we used interleaf segmentation instead (Fig. 4b). In contrast to view-sharing along k_v, which causes ghosting in the velocity direction, view-sharing among spiral interleaves introduces swirling artifacts in image domain, reducing the effective unaliased spatial field-of-view by a factor of 2. However, only moving spins (flowing blood) experience these artifacts, and vessels on the same side of the neck are relatively close to each other. Therefore, the unaliased field-of-view is wide enough to enclose all vessels on one side of the neck, so

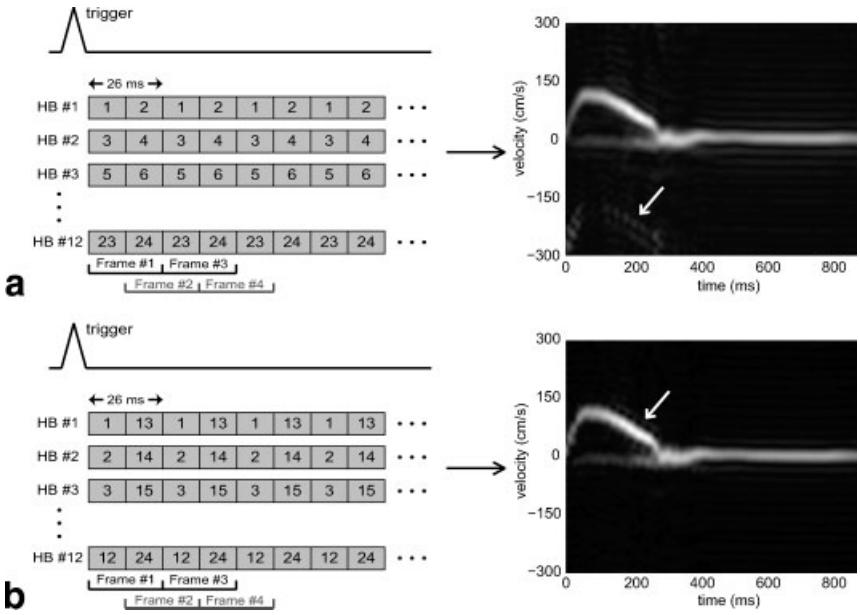

FIG. 3. Comparison of artifacts in different view-orderings, in a 12-heartbeat acquisition using single-shot spiral readouts. Each box represents the acquisition of one k_v level, during one imaging TR. A sliding window is used to produce a new image every TR. Acquiring the k_v levels in a sequential fashion (**a**), ghosting artifacts appear shifted by 1/2 of the velocity field-of-view. By acquiring them in an interleaved fashion (**b**), the artifacts overlap with the true flow profile. The aortic valve flow profiles shown are from a fully-sampled 24-heartbeat healthy volunteer acquisition, and 50% of the data was appropriately discarded to simulate the different view-orderings.

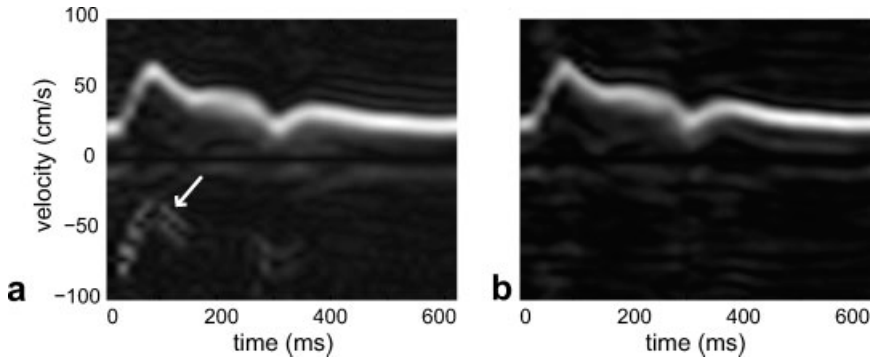

FIG. 4. Comparison of different view-orderings for multishot spiral FVE, in a healthy volunteer carotid study. When two or more k_v levels are acquired during the same heartbeat, velocity distribution changes between consecutive TRs cause ghosting artifacts along the velocity axis (**a**, arrow). This artifact is not seen if, in the same heartbeat, different spiral interleaves, but only one k_v encoding, are acquired (**b**).

that quantitation of a vessel of interest will not be disturbed by flow from neighboring vessels (e.g., measurement of flow in the left carotid arteries will not be disturbed by flow in the the left jugular vein). To suppress signal from the opposite side of the neck, we separately reconstructed data from the left and right neck-coil elements. This uses the receiver coil sensitivity profile to avoid spiral view-sharing artifacts. In the face of these observations, we used spiral interleaf view-sharing in all subsequent carotid studies.

Representative in vivo results are compared with Doppler ultrasound in Fig. 5. Large ROIs were manually specified around the entire heart and the right side of the neck, respectively, and the in-plane localization algorithm was able to successfully pin-point voxels containing the flows of interest. The MRI measured time-velocity histograms show good agreement with the ultrasound measurements, as the peak velocities and the shape of flow waveforms were comparable to what was observed in the ultrasound studies.

Figure 6 illustrates spiral FVE's ability of detecting different regions of flow from a single dataset. A different flow distribution was calculated for each voxel, and the distributions from single voxels from different ROIs are displayed. Each voxel was automatically selected within the specified ROIs, using the flow localization algorithm described previously. Red and blue dots indicate voxels where ascending and descending blood flow was detected, respectively, and the color intensity of each dot indicates the highest velocity detected in that voxel in a particular temporal frame. This sort of representation can be used by the operator to facilitate the process of manually specifying the ROI. As the data is temporally resolved, the operator can step through the cardiac cycle and visualize the different regions of flow during systole and diastole, for example. A modified in-plane localization algorithm could be designed to correct for in-plane motion of the region of interest during the cardiac cycle.

Figure 7 shows 71% and 60% improvement in velocity resolution using homodyne reconstruction along k_v, when imaging the aortic valves of a healthy volunteer (a–c) and a patient with aortic stenosis (d–f). The fully-sampled datasets (c,f) had originally 24 and 32 velocity encoding levels, respectively. Data was discarded from the positive side of k_v space and the missing data was synthesized from only 14 and 20 encoding levels using homodyne reconstruction (b,e). Full k-space results using only the central 14 and 20 k_v levels are also shown for comparison (a,d). Partial Fourier performed well in both healthy volunteer and patient studies, and no significant loss of resolution or artifacts was noticed even when discarding 42% of the data. The acquisition time could have been reduced from 12 to 7 heartbeats in the healthy volunteer study, and from 8 to 5 heartbeats in the patient study. Additionally, the

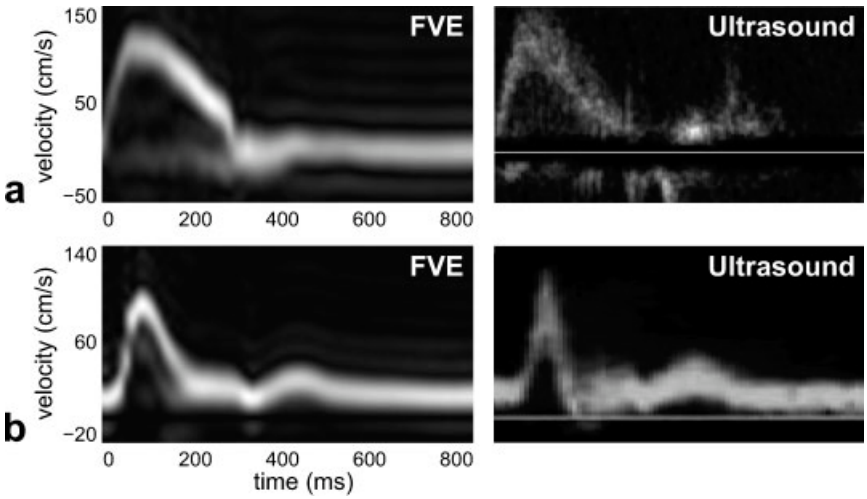

FIG. 5. Comparison of the spiral FVE method with Doppler ultrasound, in healthy volunteer studies: (**a**) aortic valve and (**b**) carotid artery. Peak velocity and time-velocity waveforms are in good agreement.

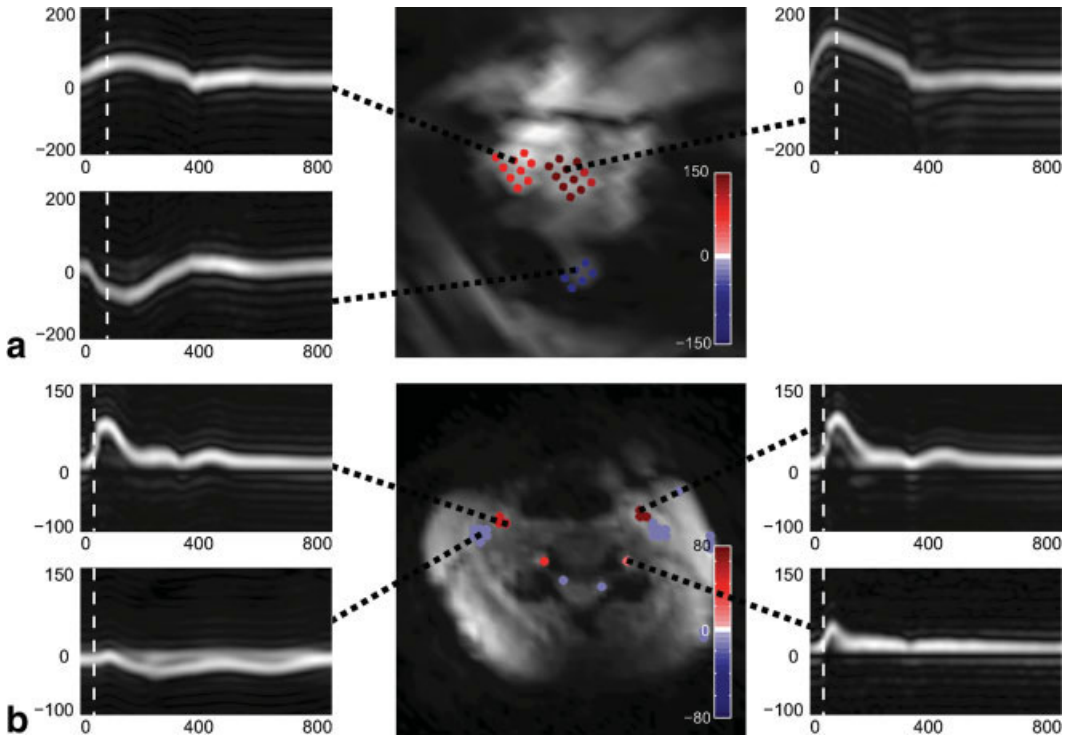

FIG. 6. Multiple flow distributions obtained from a single cardiac (**a**) and neck (**b**) dataset. For each voxel in the images, a flow distribution was calculated, and the red and blue dots indicate voxels, where ascending and descending blood flow was detected, respectively. The color intensity of each dot indicates the highest velocity detected in that voxel in a particular temporal frame (indicated by the white dashed lines). Multiple ROIs were specified around different regions of the heart and the neck, and the flow distributions from voxels automatically selected from each ROI are shown.

patient results (d–f) demonstrate that spiral FVE can accurately detect complex flow, as a high-speed jet with a wide distribution of velocities is clearly visible.

DISCUSSION

In spiral FVE, there is an important trade-off between velocity resolution, temporal resolution, and scan time. This trade-off also involves other scan parameters such as velocity field-of-view, number of spiral interleaves, spiral readout duration, spatial resolution, and spatial field-of-view. Velocity resolution can be improved in many ways, such as increasing the breath-hold duration to acquire more k_v levels, or by reducing the velocity field-of-view. Temporal resolution can be made as high as one TR duration (13 msec) by segmenting the k_v encodes across more R-R

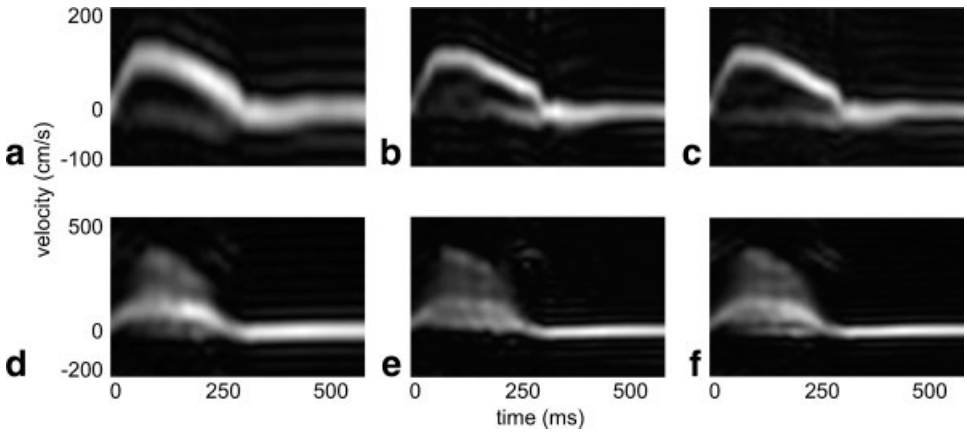

FIG. 7. Evaluation of partial *k*-space reconstruction along k_v, in aortic valve studies of a healthy volunteer (**a**–**c**) and a patient with aortic stenosis (**d**–**f**). Homodyne reconstruction performed well in both healthy volunteer (b) and patient (e) studies, improving the velocity resolution by 71% and 60%, respectively. Full *k*-space distributions with the same number of k_v samples are shown for comparison (a,d), as well as the fully-sampled datasets (c,f). Velocity resolution improvement translates to scan time reduction from 12 to 7 heartbeats, and from 8 to 5 heartbeats, respectively. Note the high-speed jet with a wide distribution of velocities in the patient data.

intervals (longer breath-holds), or by compromising velocity resolution or field-of-view. Spatial resolution can be improved by reducing the field-of-view, or by increasing the number of spiral interleaves, which would require compromising other scan parameters such as scan time, temporal resolution, and/or velocity resolution.

Artifacts and loss of temporal resolution due to view-sharing can be avoided or corrected using different approaches. Acquiring multiple k_v levels per heartbeat reduces scan time, but causes blurring along the time axis and ghosting along the velocity axis. Blurring is caused by the reduction in temporal resolution, and ghosting artifacts arise when the velocity distribution changes between the acquisition of consecutive velocity encodes (Fig. 3). Although ghosting is not seen in the multiple interleave results if appropriate view-ordering is used (Fig. 4), the temporal resolution is still lower, and this may cause blurring when the velocity distribution changes rapidly. Both ghosting and blurring can be overcome by acquiring only one view per heartbeat, but this would require increase in scan time or reduction in velocity resolution. As an alternative, these artifacts may be corrected using techniques that exploit efficient use of *k-t* space, such as UNFOLD (21) and *k-t* BLAST (22). Applications of these methods have been demonstrated to both cylindrical beam and slice-selective FVE (23,24), and similar approaches can be directly applied to spiral FVE to reduce breath-hold duration even further, without reduction in velocity or temporal resolution.

As the spiral readouts are considerably long, another potential issue in the proposed method is blurring in image domain, due to off-resonance. Because SNR was not a limiting issue for the applications we have presented, spiral FVE may perform better at lower field strengths where there is reduced off-resonance. At 3T, localized shimming and off-resonance correction techniques can be used to reduce blurring. Furthermore, readout duration can be reduced by decreasing the spatial resolution or field-of-view, or by using variable-density spirals (25,26). Another alternative is to use multiple short spiral interleaves, which would require longer scan times, but parallel imaging techniques (27,28) can potentially accelerate acquisition if multichannel receiver coils are used. This approach also has the benefit of allowing increase in the frame rate, as the number of imaged cardiac phases is limited by the minimum TR. Another possible solution to the off-resonance problem is the use of EPI trajectories, which produce different off-resonance effects (geometric warping) (29), but are also more sensitive to artifacts from in-plane flow or motion.

Another noticeable artifact in spiral FVE is Gibbs ringing. These artifacts can be less noticeable if velocity resolution is increased, which would also improve the ability to visualize features in the flow waveform and the precision to resolve the peak velocity, but would require longer breath-holds. Alternatively, the velocity resolution can be improved by using variable-density sampling along k_v (9), or partial *k*-space techniques (Fig. 7). Another approach to reducing ringing artifacts is to window the k_v samples before applying the inverse Fourier transform. However, windows with lower sidelobes generally have wider mainlobes, which would cause blurring along the velocity axis and consequent reduction in velocity resolution.

One drawback of the proposed method is the requirement of cardiac gating and breath-holding. Cardiac gating does not work well in patients with arrhythmias, and breath-holding may cause hemodynamic changes and is not possible for some patients (10). However, arrhythmia rejection (30) and respiratory gating schemes may overcome these problems, at the cost of increased scan time.

CONCLUSIONS

We have demonstrated that spiral FVE can resolve fully-localized time-velocity histograms in short breath-holds. Evaluation of cardiac aortic valve flow was performed in 12-heartbeat breath-holds, and evaluation of carotid flow was performed in 48-heartbeat scans with diagnostically useful temporal and velocity resolutions. The resulting peak velocity and velocity waveforms were accurate compared to Doppler ultrasound. Patient results show that this technique can accurately measure flow distributions in stenotic jets, detecting multiple velocities within a voxel.

It was also demonstrated that spiral FVE can resolve multiple sources of through-plane flow in a single slice acquisition, which is particularly useful when evaluating heart valves. A semiautomatic algorithm was developed for in-plane ROI selection, and can be adapted for different flows of interest. In carotid studies, spatial resolution was improved using multiple spiral interleaves. Even higher spatial resolution can be achieved in order to evaluate stenosis in smaller vessels such as the coronary arteries. We also demonstrated that partial Fourier techniques along the velocity encoding axis may be used to improve velocity resolution or shorten breath-hold duration, without introducing significant artifacts.

Preliminary volunteer and patient results indicate that the proposed method of spiral FVE may have an important role in the rapid and accurate quantitation of abnormal valvular flow, abnormal vascular flow, and congenital flow defects using magnetic resonance imaging.

ACKNOWLEDGMENTS

The authors thank Dr. Thomas Burke and Barbara Burke (Phantoms by Design Inc.), Kyunghyun Sung, Yoon-Chul Kim, Susana Perese, Gigi Youssef, Dr. Ramdas Pai, and Dr. Padmini Varadarajan for their support and collaboration.

REFERENCES

1. Winkler AJ, Wu J. Correction of intrinsic spectral broadening errors in Doppler peak velocity measurements made with phased sector and linear array transducers. Ultrasound Med Biol 1995;21:1029–1035.
2. Hoskins PR. Accuracy of maximum velocity estimates made using Doppler ultrasound systems. Br J Radiol 1996;69:172–177.
3. O'Donnell M. NMR blood flow imaging using multiecho, phase contrast sequences. Med Phys 1985;12:59–64.
4. Clarke GD, Hundley WG, McColl RW, Eckels R, Smith D, Chaney C, Li HF, Peshock RM. Velocity-encoded, phase-difference cine MRI measurements of coronary artery flow: dependence of flow accuracy on the number of cine frames. J Magn Reson Imag 1996;6:733–742.
5. Tang C, Blatter DD, Parker DL. Accuracy of phase-contrast flow measurements in the presence of partial-volume effects. J Magn Reson Imag 1993;3:377–385.
6. Mohiaddin RH, Gatehouse PD, Henien M, Firmin DN. Cine MR Fourier velocimetry of blood flow through cardiac valves: comparison with Doppler echocardiography. J Magn Reson Imag 1997;7:657–663.

7. Moran PR. A flow velocity zeugmatographic interface for NMR imaging in humans. Magn Reson Imag 1982;1:197–203.
8. Hu BS, Pauly JM, Macovski A. Localized real-time velocity spectra determination. Magn Reson Med 1993;30:393–398.
9. DiCarlo JC, Hargreaves BA, Nayak KS, Hu BS, Pauly JM, Nishimura DG. Variable-density one-shot Fourier velocity encoding. Magn Reson Med 2005;54:645–655.
10. Macgowan CK, Kellenberger CJ, Detsky JS, Roman K, Yoo SJ. Real-time Fourier velocity encoding: an in vivo evaluation. J Magn Reson Imag 2005;21:297–304.
11. Feinberg DA, Crooks LE, Sheldon P, Hoenninger III J, Watts J, Arakawa M. Magnetic resonance imaging the velocity vector components of fluid flow. Magn Reson Med 1985;2:555–566.
12. Hennig J, Mueri M, Brunner P, Friedburg H. Fast and exact flow measurements with the fast Fourier flow technique. Magn Reson Med 1988;6:369–372.
13. Galea D, Lauzon ML, Drangova M. Peak velocity determination using fast Fourier velocity encoding with minimal spatial encoding. Med Phys 2002;29:1719–1728.
14. Noll DC, Nishimura DG, Macovski A. Homodyne detection in magnetic resonance imaging. IEEE Trans Med Imag 1991;10:154–163.
15. Hargreaves BA. Spin-manipulation methods for efficient magnetic resonance imaging. Ph.D. Dissertation. Stanford: Stanford University; 2001. 131 p.
16. Zur Y, Wood ML, Neuringer LJ. Spoiling of transverse magnetization in steady-state sequences. Magn Reson Med 1991;21:251–263.
17. Jackson JI, Meyer CH, Nishimura DG, Macovski A. Selection of a convolution function for Fourier inversion using gridding. IEEE Trans Med Imaging 1991;10:473–478.
18. Riederer SJ, Tasciyan T, Farzaneh F, Lee JN, Wright RC, Herfkens RJ. MR fluoroscopy: technical feasibility. Magn Reson Med 1988;8:1–15.
19. Gao JH, Holland SK, Gore JC. Nuclear magnetic resonance signal from flowing nuclei in rapid imaging using gradient echoes. Med Phys 1988;15:809–814.
20. Bartels RH, Beatty JC, Barsky BA. An introduction to splines for use in computer graphics and geometric modelling. San Francisco, CA: Morgan Kaufmann; 1987. 476 p.
21. Tsao J. On the UNFOLD method. Magn Reson Med 2002;47: 202–207.
22. Tsao J, Boesiger P, Pruessmann KP. k-t BLAST and k-t SENSE: dynamic MRI with high frame rate exploiting spatiotemporal correlations. Magn Reson Med 2003;50:1031–1042.
23. Macgowan CK, Madore B. Application of UNFOLD to real-time Fourier velocity encoding. In: Proceedings of the 14th Annual Meeting of ISMRM, Seattle, 2006. p 872.
24. Hansen MS, Baltes C, Tsao J, Kozerke S, Pruessmann KP, Boesiger P, Pedersen EM. Accelerated dynamic Fourier velocity encoding by exploiting velocity-spatio-temporal correlations. MAGMA 2004;17: 86–94.
25. Tsai CM, Nishimura DG. Reduced aliasing artifacts using variable-density *k*-space sampling trajectories. Magn Reson Med 2000;43: 452–458.
26. Lee J, Pauly JM, Nishimura DG. Partial *k*-space for under-sampled variable-density spiral trajectories. In: Proceedings of the 11th Annual Meeting of ISMRM, Toronto, 2003. p 475.
27. Pruessmann KP, Weiger M, Bornert P, Boesiger P. Advances in sensitivity encoding with arbitrary *k*-space trajectories. Magn Reson Med 2001;46:638–651.
28. Samsonov AA, Block WF, Arunachalam A, Field AS. Advances in locally constrained *k*-space-based parallel MRI. Magn Reson Med 2006;55:431–438.
29. Feinberg DA, Oshio K. Gradient-echo shifting in fast MRI techniques (GRASE imaging) for correction of field inhomogeneity errors and chemical shift. J Magn Reson 1992;97:177–183.
30. Chia JM, Fischer SE, Wickline SA, Lorenz CH. Arrhythmia rejection using a VCG-based triggering algorithm. In: Proceedings of the 8th Annual Meeting of ISMRM, Denver, 2000. p 201.